Optimal Control Approach to Helicopter Noise Abatement Trajectories in Nonstandard Atmospheric Conditions

Hartjes, Sander; Visser, H.G.

Important note
To cite this publication, please use the final published version (if applicable).
Please check the document version above.

An Optimal Control Approach to Helicopter Noise Abatement Trajectories in Non-Standard Atmospheric Conditions

S. Hartjes* and H.G. Visser†

This paper discusses the development of a software suite which aims to optimize helicopter trajectories with respect to the noise impact on the ground. The software suite has been developed around an advanced gradient-based optimization algorithm based on optimal control theory. The helicopter trajectories are modeled using an eight degree-of-freedom flight mechanics model. To determine the noise impact on the ground, a helicopter noise model has been developed in this work which consists of three modules, viz. a helicopter source noise model, a propagation model and a noise impact model. To determine the noise levels on the ground, the source noise levels are determined from a database of aeroacoustically determined noise levels for varying flight conditions, projected on a hemisphere centered at the main rotor hub. The noise propagation model included in the suite is capable of determining the propagation loss between the source and the receiver in non-standard atmospheric conditions, and yields the total noise level in individual receiver locations. Finally, these noise levels can be quantified into a single noise impact criterion, which can be used as an optimization criterion in the optimal control formulation. To exemplify the capabilities of the suite a hypothetical city center approach procedure has been optimized for the noise impact in communities surrounding the helispot.

Nomenclature

c	=	speed of sound [m·s^{-1}]
C_T^{elem}	=	thrust coefficient in blade element theory [-]
C_T^{Gl}	=	thrust coefficient in Glauert theory [-]
F_x	=	force component along the body x-axis [N]
F_y	=	force component along the body y-axis [N]
F_z	=	force component along the body z-axis [N]
g	=	speed of sound gradient [s^{-1}]

*Assistant Professor, Faculty of Aerospace Engineering, Delft University of Technology, P.O. Box 5058, 2600 GB, Delft, The Netherlands.
†Associate Professor, Faculty of Aerospace Engineering, Delft University of Technology, P.O. Box 5058, 2600 GB, Delft, The Netherlands, Associate Fellow AIAA.

I_x = helicopter moment of inertia about the body x-axis [kg·m^2]

I_y = helicopter moment of inertia about the body y-axis [kg·m^2]

I_z = helicopter moment of inertia about the body z-axis [kg·m^2]

J_{xz} = helicopter product of inertia about the body x- and z- axes [kg·m^2]

k = wave number [rad·m^{-1}]

L = helicopter roll moment [N·m]

M = helicopter pitch moment [N·m]

m = helicopter mass [kg]

N = helicopter yaw moment [N·m]

p = helicopter roll rate [rad·s^{-1}]

q = helicopter pitch rate [rad·s^{-1}]

Q = reflection factor [-]

r = helicopter yaw rate [rad·s^{-1}]

R = ray path radius of curvature [m]

s = ray path length [m]

u = helicopter airspeed component along the body x-axis [m·s^{-1}]

v = helicopter airspeed component along the body y-axis [m·s^{-1}]

w = helicopter airspeed component along the body z-axis [m·s^{-1}]

u_w = wind speed component along the body x-axis [m·s^{-1}]

v_w = wind speed component along the body y-axis [m·s^{-1}]

V_{w_x} = wind speed component along the Earth-fixed x-axis [m·s^{-1}]

V_{w_y} = wind speed component along the Earth-fixed x-axis [m·s^{-1}]

w_w = wind speed component along the body z-axis [m·s^{-1}]

θ = ray path angle of incidence [rad]

Θ = helicopter pitch angle [rad]

λ_i = non-dimensional uniform induced downwash [-]

Φ = helicopter roll angle [rad]

Ψ = helicopter yaw angle [rad]

τ_{λ_i} = time constant of response [-]

Subscripts

mr = main rotor

tr = tail rotor

I. Introduction

Although a less common sight then fixed-wing aircraft, helicopters offer specific abilities to execute specialized missions, but, consequently, also offer different challenges in terms of the environmental impact. The relatively small number of helicopters in operation may result in a negligible global environmental impact as compared to fixed-wing traffic. However, the specific types of operations helicopters are used for often imply that they operate in close proximity to population, and as such can significantly contribute to the local impact on the human environment, especially when noise nuisance is considered. This is further exacerbated by the predicted growth in helicopter deliveries with new or increased operations in the corporate sector, emergency medical services and commercial transport.

To mitigate the impact different approaches exist which have been extensively researched. The advancement of main rotor blade development has significantly improved helicopter efficiency, but has also positively affected the noise generated at the source. Developments such as AgustaWestland's (now Leonardo Helicopters) BERP IV [?] rotor blade and Eurocopter's (now Airbus Helicopters) Blue Edge™[?] blades have been shown to result in lower source noise levels, specifically by reducing the noise caused by the so-called Blade-Vortex Interaction (BVI) in slow, descending flight. Alternative tail rotor concepts such as the NOTAR system [?] developed by Hughes Helicopters and the Sud Aviation's Fenestron system [?] have also contributed to the reduction in source noise levels. The developments mentioned above all positively affected the efficiency of helicopters, and have helped reduce the impact of helicopter operations on the human environment. To bring further changes in the development of helicopters – with a strong focus on environmental impact – the European Union initiated the Clean Sky Joint Undertaking (JTI) in 2008 to advance towards the environmental goals set by the Advisory Council on Aviation Research and Innovation in Europe (ACARE) *. As part of the Clean Sky JTI, the Green Rotorcraft (GRC) Integrated Technology Demonstrator (ITD) program aims to develop a new generation of helicopters that, amongst others, leads to a reduction of 25% in carbon dioxide emissions and a reduction of the noise footprint area by 50%. These objectives are to be realized by 2020, with the helicopter fleet of 2000 serving as a baseline. Although the design of new rotorcraft plays an important role in GRC, specifically the mitigation of the noise impact is expected to be achieved by the development of new procedures, which is the focus of this study.

Research into noise abatement procedures has been quite extensive. At the German Aerospace Center (DLR) a combination of measured and computationally derived noise levels has been used to predict noise footprints in arrival procedures [? ? ?]. Helicopter trajectories can be modeled by a number of control points which can in turn be optimized using an evolutionary algorithm in aiming to reduce the noise footprint. A similar approach, now based on computationally derived noise models, was used by AgustaWestland [?]. In this study the evolutionary algorithm was combined with a gradient-based method for local refinement of the solutions. Essentially the problems considered here are trajectory optimization problems, for which the application of optimization based on optimal control theory can

---

*http://www.acare4europe.org/documents/vision-2020

be shown to be the most efficient approach [**?**]. These methods have been applied in a number of studies regarding helicopter operations. Although not focusing on noise abatement, Zhao [**?**], Jhemi [**?**], Okuno [**? ?**] and Bottasso [**?**] have all shown the capabilities of optimal control-based optimization techniques for solving complex trajectory optimization problems for rotorcraft. Tsuchiya [**?**] used similar techniques to reduce the noise footprint, and, finally, Visser [**?**] has already considered community noise impact as an optimization criterion, albeit that the latter two studies used relatively simple rotorcraft noise models.

Previous research has shown several approaches towards the development of green rotorcraft trajectories. This study aims to overcome some of the limitations of optimal control-based studies, mainly by integrating higher-fidelity models and by using an advanced optimization algorithm. In this approach, the optimization method developed in this study combines the efficiency of an optimization algorithm based on optimal control theory with higher-fidelity models to model the helicopter flight dynamics (as compared to previous optimal control-based studies) and the noise impact on the ground. For this purpose the European Clean Helicopter Optimization (ECHO) software suite was developed [**? ? ?**]. The suite combines an advanced optimization algorithm with a rigid-body flight dynamics model, a source noise model, a noise propagation model and a Geographic Information System (GIS) containing local population data. This permits the optimization of helicopter trajectories with respect to a number of generic and site-specific noise criteria in a 3-dimensional environment. To exemplify the capabilities of the ECHO suite, an approach trajectory to a helispot in Rotterdam city center has been optimized for the noise impact on the ground and for flight time.

The structure of this paper is as follows. First, the numerical optimization methodology is presented, followed by an overview of the helicopter flight dynamics and the noise model in sections III and IV, respectively. Next, an example scenario is introduced including its results, followed by the conclusions and recommendations in Section VII.

II. Numerical Methodology

The core of the ECHO suite consists of a gradient-based optimization algorithm based on optimal control theory. ECHO uses a direct solution method based on global pseudospectral collocation based on Radau quadrature. This method is available through the General Pseudospectral Optimization Software (GPOPS) [**?**]. The principle of this method is that the continuous time problem is first transcribed to a finite-dimensional Non-Linear Programming (NLP) problem. To achieve this, the time interval is discretized to a sequence of smaller intervals based on the requirements for Radau quadrature. The vehicle states and control variables at the nodes – the points delimiting the sub-intervals - are then treated as variables in the NLP formulation. The system differential equations are then integrated explicitly using Radau quadrature – a form of Gaussian quadrature. These are collocated to equal the local approximation of the state variables (and their first derivatives) at the nodes. Finally, path and boundary constraints are expressed as algebraic equations and treated as constraints in the NLP formulation.

Following the method described above the original continuous time problem is transformed to a large-scale NLP

problem which is solved with the numerical solver SNOPT [**?**]. SNOPT is capable of solving large-scale NLP problems in a relatively short time by making use of the sparsity of the NLP problem.

The use of a direct solution method does, however, require the problem formulation to be a set of continuous functions, preferably up to the first derivative. As such, although some exceptions may prove acceptable, all equations contributing to the problem should be smooth differentiable functions. To provide the gradients of the problem formulation GPOPS offers several different, integrated options. Although providing analytical gradients results in the best accuracy and the lowest computational effort, differentiating and coding the derivatives for all models involved is certainly no trivial task. To balance runtime and accuracy, for the flight dynamics model and the noise model the automatic differentiation tool Auto_Deriv [**?**] was used. The gradient information results in very fast convergence and, consequently, relatively short runtimes, but does require extra attention in the selection or definition of models used in the problem formulation. Furthermore, the method requires a single performance index to be defined. To still allow for multiple optimization criteria, a composite performance index can be formulated as follows:

$$J = \sum_{n=1}^{N} k_n j_n + \sum_{m=1}^{M} k_m \int_{t_0}^{t_f} j_m dt \tag{1}$$

where the parameters k_n and k_m are weighting factors ($0 \leq k_{n,m} \leq 1$) for j_n and j_m, respectively, which are the optimization criteria. The first term depicts the endpoint or Mayer cost, and the second part defines the running or Lagrange cost component. This formulation of the objective function allows the optimization with respect to a weighted sum of different criteria.

Although the optimization method used in this work does not generally allow for discontinuities in the problem formulation, GPOPS allows for a multi-phase definition of the problem. This in essence means that a set of piecewise continuous problems can be solved which are linked at the so-called switching points. Although each of the sub-problems is required to be continuous, at the switching points discontinuities in the system dynamics are allowed.

III. Helicopter Flight Dynamics

To model the free motion of the helicopter, an eight degree-of-freedom rigid-body dynamic model with quasi-steady inflow of the main and tail rotor has been integrated in the ECHO suite. The model, based on the work by Pavel [**?**] consists of fourteen state variables ($u, v, w, p, q, r, \Phi, \Theta, \Psi, x, y, z, \lambda_{i_{mr}}, \lambda_{i_{tr}}$) representing the airspeed components, body angular rates and angles, position and inflow angles. The helicopter is controlled using the collective pitch angle θ_0, the longitudinal and lateral cyclic angles θ_{1s} and θ_{1c}, and, finally, the tail rotor collective pitch angle, θ_{tr}. The equations of motion can then be expressed as follows:

$$\dot{u} = \frac{F_x}{m} - q(w + w_w) + r(v + v_w) - \dot{u}_w \tag{2}$$

5

$$\dot{v} = \frac{F_y}{m} - r\left(u + u_w\right) + p\left(w + w_w\right) - \dot{v}_w \tag{3}$$

$$\dot{w} = \frac{F_z}{m} - p\left(v + v_w\right) + q\left(u + u_w\right) - \dot{w}_w \tag{4}$$

$$\dot{p} = \frac{\left(L - \left(I_z - I_y\right)qr + J_{xz}\left(\dot{r} + pq\right)\right)}{I_x} \tag{5}$$

$$\dot{q} = \frac{\left(M - \left(I_x - I_z\right)rp - J_{xz}\left(p^2 - r^2\right)\right)}{I_y} \tag{6}$$

$$\dot{r} = \frac{\left(N - \left(I_y - I_x\right)pq + J_{xz}\left(\frac{\left(L-\left(I_z-I_y\right)qr+J_{xz}pq\right)}{I_x} - rq\right)\right)}{I_z - \frac{J_{xz}^2}{I_x}} \tag{7}$$

$$\dot{\Theta} = q\cos\Phi - r\sin\Phi \tag{8}$$

$$\dot{\Psi} = \frac{\left(q\sin\Phi + r\cos\Phi\right)}{\cos\Theta} \tag{9}$$

$$\dot{\Phi} = p + \dot{\Psi}\sin\Theta \tag{10}$$

$$\dot{\lambda}_{i_{mr}} = \frac{C_{T_{mr}}^{elem} - C_{T_{mr}}^{Gl}}{\tau_{\lambda_{i_{mr}}}} \tag{11}$$

$$\dot{\lambda}_{i_{tr}} = \frac{C_{T_{tr}}^{elem} - C_{T_{tr}}^{Gl}}{\tau_{\lambda_{i_{tr}}}} \tag{12}$$

$$\dot{x} = \left[u\cos\Theta + \left(v\sin\Phi + w\cos\Phi\right)\sin\Theta\right]\cos\Psi - \left(v\cos\Phi - w\sin\Phi\right)\sin\Psi + V_{w_x} \tag{13}$$

$$\dot{y} = \left[u\cos\Theta + \left(v\sin\Phi + w\cos\Phi\right)\sin\Theta\right]\sin\Psi + \left(v\cos\Phi - w\sin\Phi\right)\cos\Psi + V_{w_y} \tag{14}$$

$$\dot{z} = -u \sin \Theta + (v \sin \Phi + w \cos \Phi) \cos \Theta \qquad (15)$$

One of the disadvantages of the selected optimization method in combination with the above dynamic model is the potential occurrence of so-called bang-bang control. These excessive control rates can occur when the objective function and the equations of motion are linear in the control variables. However, since the current problem formulation does not allow to explicitly constrain the control rates, so-called pseudo-controls are introduced. To this end, the four original control variables are considered as state variables, and their derivatives are used as the control variables in the problem formulation. Although these derivatives may not have a direct physical meaning, they can be constrained, or, as was done in this study, a control penalty can be applied. For this purpose, the control rates are squared and added to the objective function of Eq. (1). The objective function then becomes:

$$J = \sum_{n=1}^{N} k_n j_n + \sum_{m=1}^{M} k_m \int_{t_0}^{t_f} j_m dt + \alpha \int_{t_0}^{t_f} \sum_{i=1}^{4} u_i^2 dt \qquad (16)$$

Here, α is a weighting factor. By choosing a very small value for α the objective function is no longer linear in the controls, whilst the contribution of the control penalty to the objective value itself is negligible. The introduction of pseudo-controls leads to a total of eighteen state variables and four control variables.

In the case studies presented in this paper, the parameters describing a Messerschmitt-Bölkow-Blohm (MBB) Bo-105 helicopter have been used. To ensure flight within the flight envelope, and to ensure passenger comfort, a number of path constraints have been imposed that are applied to all cases. These can be found in Table 1.

Table 1   General problem constraints

Constraint	(In)equality
True airspeed	$30 \leq V \leq 100 \ kts$
Vertical speed	$-1000 \leq \dot{z} \leq 0 \ fpm$
Acceleration	$-2 \leq \dot{V} \leq 0 \ kts \cdot s^{-1}$
Vertical acceleration	$|\dot{w}| \leq 0.3 \ g$
Roll angle	$|\Phi| \leq 25°$
Flight path angle	$0° \leq \gamma \leq 10°$

IV. Noise Modeling

As opposed to fixed-wing aircraft that generally operate in less densely-populated areas and where the frequency of movements is a main driver for annoyance in near-airport communities, helicopters often operate in densely populated areas, and as such each individual operation can significantly contribute to the noise annoyance near the helispot. In addition, helicopter noise is specifically difficult to model accurately. Firstly, the source noise is highly dependent on

maneuvering. For instance High Speed Impulsive (HSI) noise and especially Blade Vortex Interaction (BVI), which occurs typically in low speed descent, generally result in significantly higher source noise levels and are considered annoying to ground-based observers. Furthermore, helicopter source noise is highly asymmetric due to the different local airspeeds at the advancing and retreating blades. To account for these effects and accurately predict the source noise levels, the ECHO suite contains a database model containing source noise levels assuming steady-state flight conditions. Data is available for a limited number of different flight conditions and frequencies, and the database has been determined specifically for the Bo-105 helicopter used in this study. The source noise levels are projected onto hemispheres fixed to the main rotor hub, and are always defined as parallel to the ground plane. The hemispheres only rotate about the Earth-fixed z-axis along with helicopter yaw. In total datasets for twelve different steady-state flight conditions are available, viz. for three different airspeeds ($V = [30, 65, 100]$ knots) and four different flight path angles ($\gamma = [-10°, -7.5°, -5°, 0°]$), and each set contains the source noise levels for the first twenty blade passage frequencies (BPF). Data is available on 145 locations on the hemisphere surface, which corresponds to a data point at 15° increments of both the azimuth and elevation angle. The database is created offline and requires the control settings derived from a trim solver as input.

The trim conditions for steady state flight serve as the input for the aeroelastic solver [? ? ?], which is used to determine the blade body pressures combines a blade structural dynamics model and an unsteady aerodynamic solver. The blade structural dynamics are modeled using a beam-like based on a non-linear bending-torsion formulation. The structural displacements are used as inputs for the aerodynamic solver, which consists of a potential-flow, free-wake Boundary Element Method (BEM) solver. The wake of the rotor is divided in two parts: the near, potential wake is close to the trailing edge of the blade and cannot come in contact with any of the following wakes. The far, vortex wake uses a zero-thickness wake with thick Rankine vortices. The resulting pressure distribution can then in turn be used to update the elastic deformation in the blade structural model. The body pressure determined by the aerodynamic solver are also used to determine the acoustic field using a Ffowcs-Williams and Hawkings formulation [?], in turn solved by a Farassat formulation [?].

The resulting acoustic field is projected on a hemisphere with a radius of 150 m centered at the rotor hub to ensure the hemisphere lies in the far field of the noise source. It should be noted that the hemispheres were constructed under the assumption of a non-refracting atmosphere. However, in reality, sound rays can already be refracted between the source at the rotor hub and the hemisphere itself. To account for this, the hemispheres can be propagated backwards to 1 m from the source by assuming only a spherical spreading loss, hence by adding $20 \log_{10} (150)$ to the source noise levels. This places the hemisphere at 1 m from the actual source, and refraction effects within this distance can be considered negligible. Only main rotor noise is included in the model, and the effect of the fuselage is not taken into account. To obtain the source noise levels for intermediate flight conditions at the nodes a linear interpolation between the sets of hemispheres is applied. The use of hemispheres and linear interpolation do not fully comply with the requirements

imposed by the use of optimal control theory. The linear interpolation has shown not to be affecting the convergence of the optimization; as mentioned above, continuity in the models and their derivatives is preferred, but not always required. The fact that hemispheres were used could indicate that some sound rays are launched upward with respect to the rotor hub – where no source noise is available – hence resulting in discontinuities in the objective function. However, sound rays launched upward generally travel long distances before reaching the ground, and therefore lose most of their energy. The resulting sound levels are well below the threshold values used to quantify the noise impact in this study, and therefore do not contribute to the objective function. The path constraints presented in Table 1 ensure operations within the limits of the acoustic database.

The first step in determining the noise impact of a helicopter trajectory is to determine the source noise level that is transmitted to an individual observer location, and the propagation loss between the source and the receiver. In both cases first the path of the sound rays through the atmosphere needs to be determined. In typical ray-tracing approaches [? ?], Snell's law of refraction is integrated for an infinitesimally small time step dt and assuming a constant speed of sound – and hence a straight ray path – during each step. In the approach used in this study, however, a ray path is found through a geometric ray-tracing algorithm, in an effort to reduce the computational time. In this algorithm it is assumed that the gradient of the speed of sound (rather than the speed of sound itself) is constant in an integration step. This allows for a significantly smaller number of integration steps, and in fact it has been shown [?] that for most non-standard atmospheric conditions approximately ten layers of constant speed of sound gradient (and hence ten integration steps) leads to sufficiently accurate results. It should be noted here that by discretizing the atmosphere in vertical layers only, refraction is only modeled in the vertical plane. To more accurately approximate the speed of sound gradient – especially near the ground where the wind velocity approaches zero – a logarithmic distribution of the layers has been used. Rather than accounting for refraction at the transition between two consecutive integration steps, refraction is accounted for within each layer. The ray path in each layer can then be constructed by first determining the radius of curvature for a given launch angle θ_0 as follows (see Fig. 1):

$$R_i = \frac{-c_i}{g_i \cos \theta_{0,i}} \tag{17}$$

where c_i is the speed of sound at the start of the layer, g_i is the gradient of the speed of sound and $\theta_{0,i}$ is the incidence angle at the start of the layer, defined as zero parallel to the ground plane and positive downward. The center of curvature can then be found through:

$$x_{c,i} = x_{0,i} + R_i \sin \theta_{0,i} \tag{18}$$

$$z_{c,i} = z_{0,i} + R_i \cos \theta_{0,i} \tag{19}$$

9

where $(x_{0,i}, z_{0,i})$ are the coordinates where the ray path enters the layer. Here, z is defined as positive upwards and x is positive in the distance of travel. The final incidence angle, final position and path length in the ith layer are then defined as:

$$\theta_{f,i} = \cos^{-1}\left(\frac{z_{c,i} - z_{f,i}}{R_i}\right) \qquad (20)$$

$$x_{f,i} = x_{c,i} - R_i \sin\theta_{f,i} \qquad (21)$$
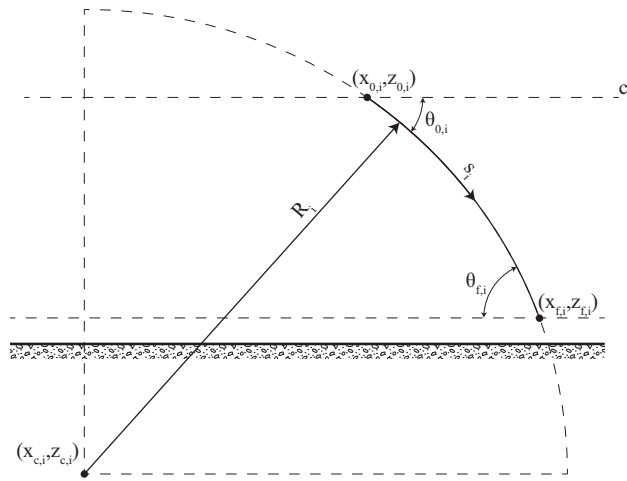
$$s_i = |R_i\left(\theta_{f,i} - \theta_{0,i}\right)| \qquad (22)$$

Fig. 1   Refraction in a linear speed of sound profile [?]

Integrating over the full distance between source and receiver then yields a refracted ray path. The layers can be selected such that the approximated speed of sound profile closely matches the real profile. The construction of the ray path between the source at the rotor hub and a receiver can then be used to determine the azimuth and elevation angles at which the ray crosses the hemisphere, which in turn yields the source noise level $SPL_{n,f}$ for all twenty BPFs.

The propagation loss can also be determined from the ray paths. Three effects are accounted for: firstly, atmospheric attenuation [?] depends on the ray path length and the temperature and humidity pattern along the path, and is directly integrated along the ray path. Secondly, the spreading loss accounts for the sound energy being spread over an increasingly larger surface at increasing distances from the source. In a refracting atmosphere ray paths may converge or diverge, leading to deviations in the spreading loss as compared to spherical spreading [?]. It can be shown that for ray path construction with relatively low wind speeds the total spreading loss can be expressed as the sum of the spherical spreading loss and a correction for focusing as follows [?]:

10

$$\Delta SPL_S = -10 \log_{10}\left(\frac{\gamma_r}{\gamma_u}\right) + 20 \log_{10}\left(\frac{s_0}{s_r}\right) \tag{23}$$

where γ_r and γ_u are the distances between two points on the ray paths at a specific time t (see Fig. 2) in a refracting and non-refracting atmosphere, respectively. The second term is the spherical spreading loss over a distance $s_r - s_0$. Although the geometric ray-tracing method does not directly yield the travel time needed to ensure both rays are evaluated at the same time t, this can be easily derived by integrating the reciprocal of the speed of sound with respect to the ray path length [?].
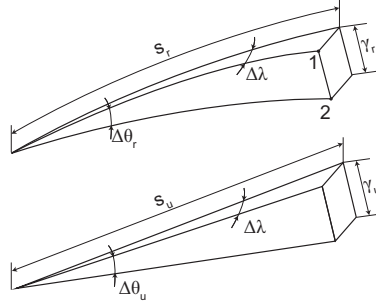

Fig. 2   Ray tube geometry [?]

Finally, a ground reflection correction is applied which accounts for the gains or losses associated with a direct and an indirect ray (reflected by the ground surface) reaching the observer, causing a phase change. It can be shown that the gain or loss due to an indirect ray reaching the observer can be expressed as [?]:

$$\Delta SPL_G = 20 \log_{10}\left|1 + \frac{s_1}{s_2} Q e^{ik(s_2 - s_1)}\right| \tag{24}$$

where k is the wave number, and s_1 and s_2 are the ray path lengths of the direct and indirect ray, respectively. The reflection coefficient Q is determined from the method defined by Delany and Bazley [?] and accounts for the ground surface type. Although multiple reflections off the ground could occur, leading to multiple indirect rays reaching the observer, this effect is not taken into account. In addition, the two rays have a different travel time and hence a different transmission time, and, consequently, will have a different noise level at the source. However, considering that the difference in travel time between both rays is very small, this effect is considered negligible, and the rays are assumed to have been launched at the same time.

The source noise and propagation models discussed above comply with the continuity constraints imposed by the direct method for optimal control for most observer locations. However, at the transition to the shadow zone, i.e. the area where no direct sound rays can reach the ground as the rays are refracted away from the ground, a discontinuity in the sound levels still occur. Although the sound levels within the shadow zone itself are sufficiently low to be disregarded when considering community noise impact, it is critical to determine the location of this transition and to

ensure continuity in the noise calculations in all observer locations. To determine the position of the shadow zone, first the lowest atmospheric layer with a negative speed of sound gradient is identified, and the final incidence angle is then assumed to be zero. Then, the process described by Eqs. (17)-(21) is reversed to determine the distance between the source and the start of the shadow zone. To ensure continuity within the shadow zone, the approach developed by Arntzen [?] has been included in the noise model. This method provides an estimate of the sound energy loss at the transition from the illuminated zone to the shadow zone, and also predicts the additional propagation within the shadow zone, based on the results of a Fast-Field Program (FFP) reference [†]. The method predicts a linear loss of up to 30 dB in the transition zone based on the local speed of sound gradient and over the remaining distance to the receiver within the shadow zone itself only atmospheric attenuation and spherical spreading losses are applied.

The total propagation loss is then subtracted from the source noise levels and an A-weighting filter is applied. This yields twenty Sound Pressure Levels (SPL) (one for each BPF) on the ground, which are in turn aggregated to obtain the A-weighted sound level L_A. This process is then repeated for all the nodes in the trajectory discretization to yield the time history $L_A(t)$ in each observer location. This can, finally, be integrated using the same method as used for the system dynamics to yield the A-weighted Sound Exposure Level (SEL), which is the noise metric used to further quantify the noise impact.

Although the previous steps allow to quantify the noise levels in individual observer locations, to assess the total impact of a full helicopter trajectory one further step is required. For this purpose, the ECHO suite includes three options to express the local noise impact in a single value which can in turn be used in the objective function of Eq. (1). The first criterion, contour area A_y, essentially counts the number of grid cells above a user-defined threshold value y of SEL. This criterion is generic as it is independent of the local population distribution. To also include the noise impact on local communities, the same principle can be used to determine the number of people exposed P_y to a certain level y of SEL. With the availability of a Geographic Information System (GIS) which contains population distribution data, the number of people being exposed to a certain threshold value of SEL can be determined and minimized. This option discretely counts the people exposed; i.e. people are either exposed or not exposed to a value higher than or equal to the threshold value. To also account for the actual value of the SEL, finally also a dose-response relationship is available which determines the maximum percentage of expected awakenings N_A due to a single nighttime flyover. The relationship was defined by the Federal Interagency Committee on Aviation Noise (FICAN) [?] and can be expressed as follows:

$$\%A = 0.0087 \left(SEL_{indoor} - 30 \right)^{1.79} \tag{25}$$

where SEL_{indoor} is the SEL calculated by the noise model minus 20.5 dB to account for the sound absorption of a

---

[†]ESDU 04011: Prediction of sound attenuation in a refracting turbulent atmosphere with a Fast Field Program

typical home [?]. This relationship -– in combination with the population data in the GIS — allows to determine and minimize the total number of awakenings due to a single helicopter operation.

V. Example Scenario

To exemplify the capabilities of the ECHO suite, an arrival to a city center helispot in the city of Rotterdam has been modeled. The helicopter approaches from the west originating from a point 18.6 km west and 1.2 km north of the helispot. This location lies above an uninhabited harbor area, which ensures the noise criterion is not dependent on the starting conditions. The helicopter lands at a helispot with an elevation of 120 ft. The problem is formulated with two phases: the arrival phase essentially connects an en-route segment – not modeled in this example – to the approach phase in which the helicopter prepares for landing. The arrival phase starts at an altitude of 3,000 ft Above Ground Level (AGL) at a true airspeed of 100 kts and in level flight $(v_{z_0} = 0)$. The phase ends at 1,000 ft AGL. Due to the presence of high-rise buildings close to the helispot, the final heading during the arrival phase needs to be either 66° or 246° -– depending on the direction of the wind -– to ensure the helicopter is correctly aligned with the helispot. In the approach phase the helicopter descends further to the helispot whilst maintaining its heading. It is assumed that a vertical landing is executed at the helispot. The landing itself is not modeled as the landing procedure itself is strictly defined due to ensure safe operations, and hence leaves no room for optimization. Consequently, the simulation ends at 150 ft Above Helipad Elevation (AHE) at a speed of 30 kts.

The problem is discretized using 60 nodes — 45 for the arrival and 15 for the approach, yielding an NLP-problem with 1,485 nonlinear variables and 1,630 nonlinear constraints. The sound impact is calculated on a grid of 54x46 km with cells of 1x1 km. The 2,484 grid cells contain a total of 2.7 million people. An overview of the procedure and the surrounding area can be seen in Fig. 3.

Fig. 3   Scenario overview

The resulting problem can be optimized for either of the three aforementioned noise criteria, flight time and total fuel burn, or any combination thereof. The objective function for the optimal control formulation can then be defined in line with Eq. (1) as follows:

$$J = k_1 t_f + k_2 \int_{t_0}^{t_f} \dot{m}_f dt + k_3 A_y + k_4 P_y + k_5 N_A \tag{26}$$

where t_f is the total flight time and $\dot{m}_f$ is the mass flow of fuel. The latter is determined through a generic model dependent only on the engine power required, which is provided by the Swiss Federal Office for Civil Aviation (FOCA) [‡]. It should be noted that in all example cases only one or two of the criteria are included in the objective function at the same time.

For this problem the typical execution time at a standard laptop CPU is around 30 seconds when noise is not included, and 5-60 minutes when noise is included, depending on the availability of a good initial guess. To obtain an initial guess two steps have been used. First, a simple, minimum time problem is defined in which the initial guess is manually defined. This guess consists only of the start and end points of the trajectory. For the predefined initial and final conditions their respective values have been used, other variables have been set to zero; the GPOPS program has shown to be sufficiently robust to obtain an optimal trajectory from this guess. This simple but complete minimum time trajectory is then used to initialize further optimizations involving different criteria.

The possibility of non-convexity of the objective function – mainly caused by the population distribution – may lead to local minima. A typical means to identify the existence of local minima is by numerical trials initialized with widely varying initial guesses for the trajectory solution. This approach has been used to test for local minima in this study as well, but it has been found that all alternative initial guess solutions result in the same solution.

VI. Results

To give a first impression of the capabilities of the ECHO suite, the scenario defined above has been optimized in ISA conditions with respect to flight time ($k_1 = 1$) and parametrically varied weighting factors for the awakenings ($0 \leq k_5 \leq 0.2$). The other weighting factor are zero ($k_{2-4} = 0$). Table 2 shows the results for some of the values of k_5 that have been evaluated. Figures 4 and 5 show the ground tracks and airspeed and altitude profiles. Finally, Fig. 6 shows the 50, 60 and 70 dBA SEL contours to exemplify how the trajectory is shaped to reduce the noise impact on the population.

Table 2   Results in ISA

Case	Objective	t_f [s]	Δt_f [%]	N_A	ΔN_A [%]
C01	t_f	367.3	n/a	3479	n/a
C02	$t_f + 0.04 N_A$	376.3	+2.46	2156	-38.0
C03	$t_f + 0.1 N_A$	389.9	+6.14	1882	-45.9

The results for the minimum time case C01 can be readily explained: a high speed is maintained, and the shortest

---

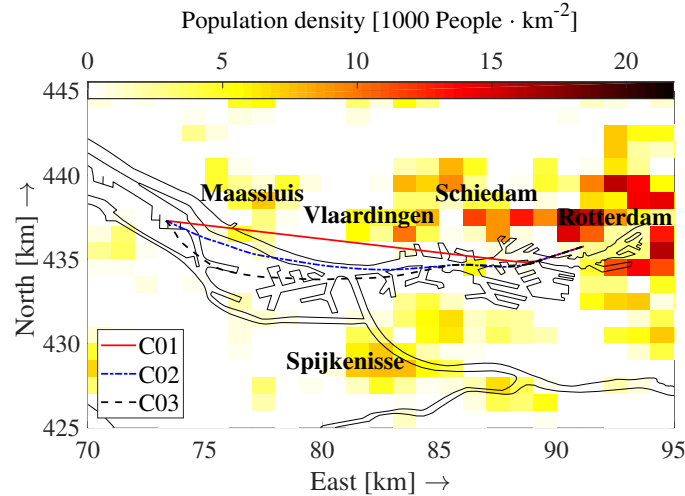[‡]available from: https://www.bazl.admin.ch
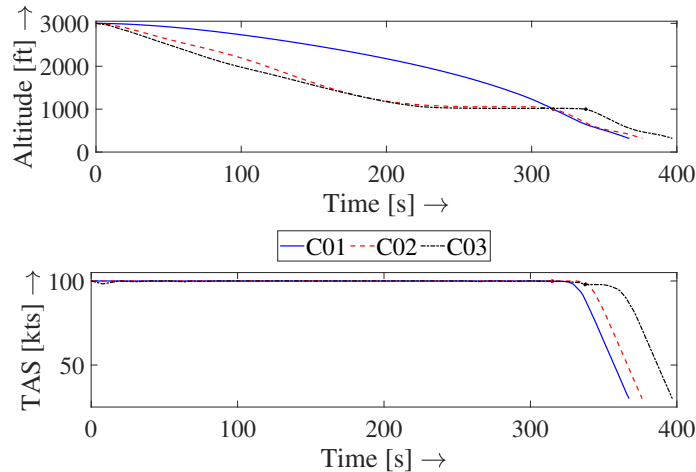
Fig. 4   Ground tracks, ISA

Fig. 5   Altitude and airspeed profile, ISA

possible path is followed. Only when required to meet the final conditions, the helicopter starts decelerating.

When, however, noise impact is included in the objective function, the trajectories change quite significantly. Firstly, it can be seen from Fig. 4 that the ground track is shifted away from populated areas, and, in fact, the helicopter flies over the Meuse river avoiding directly passing over populated areas. However, following the river in itself does not reduce the noise impact significantly, as many residential buildings are close to the waterfront. The potential reduction in noise impact of up to 46% that was identified can only be explained by also considering the altitude profile. What can be seen in Fig. 5 is that a gradual descent is initiated at the start of the trajectory, and that the second part of the trajectory is flown at the lowest allowed altitude of 1,000 ft. This behavior can be explained by considering both the source noise levels and the noise propagation effects accounted for in this study. Firstly, as the helicopter flies low, the slant range and incidence angle with respect to the observers is reduced. The first results in a lower loss in sound energy
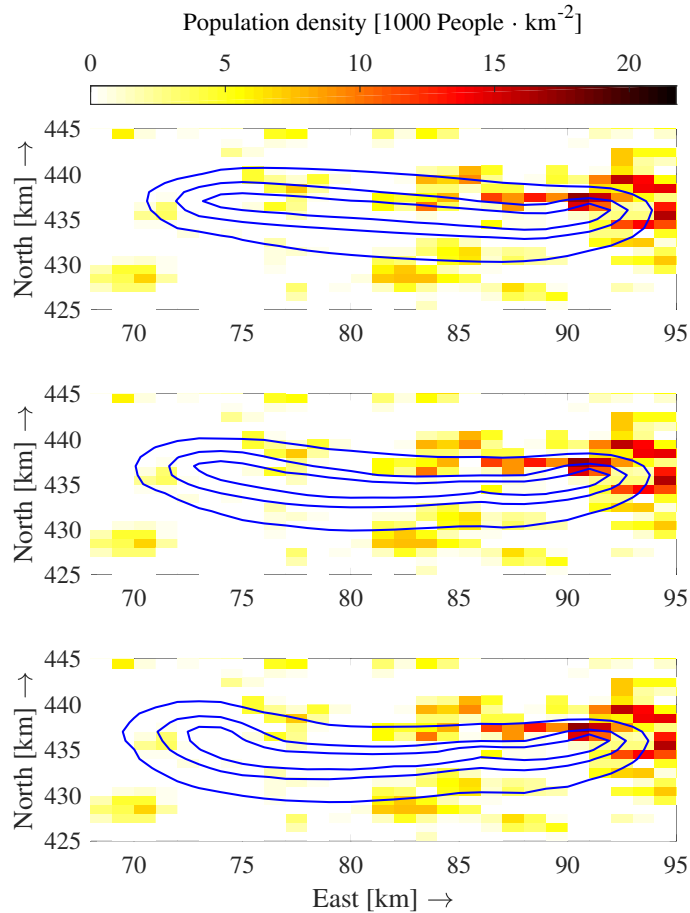
15

Fig. 6   50, 60 and 70 dBA SEL contour levels for cases C01, C02 and C03

due to absorption, whilst the former increases the lateral attenuation due to mainly the ground effect. In Fig. 7, showing the sideline noise levels for different flight altitudes, it can clearly be seen that the lateral attenuation is dominant in all but the communities directly below the helicopter. The high noise exposure directly below the helicopter mostly affects the river and the areas directly surrounding it. The combination of flying low and shifting the peak loads directly below the helicopter away from noise-sensitive areas is the main contributor to the noise impact reduction. In addition to the propagation losses the flight conditions also result in relatively low source noise levels. A high airspeed is maintained throughout the arrival phase avoiding BVI noise and reducing the exposure time which in turn leads to lower SEL values. Although the high speeds could result in HSI noise, this mostly affects the tip path plane of the main rotor blades, and mostly in a forward direction [?]. Consequently, HSI noise is assumed to not significantly affect the observer locations. In addition, the initial descent at the start of the trajectory is relatively shallow, again to avoid BVI noise affecting the communities of Maassluis and Rozenburg.

As mentioned above, the sound propagation model in the ECHO suite allows to evaluate non-standard atmospheric conditions. To exemplify this, the previous example is extended with a wind vector blowing from the East with increasing
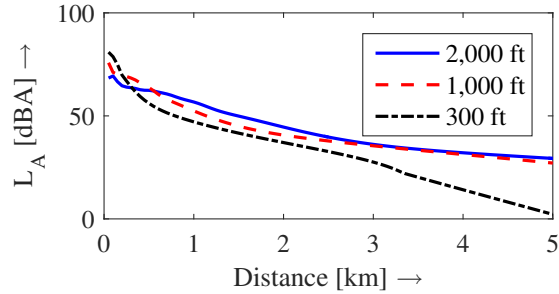
Fig. 7   Sideline noise levels

wind speeds up to 15 kts. A logarithmic wind profile is used and the wind speed V_w is expressed at 10 m altitude. The major results can be found in Table 3.

Table 3   Results for increasing headwind

Case	Objective	V_w [kts]	t_f [s]	Δt_f [%]	N_A	ΔN_A [%]
C01	t_f	0	367.3	n/a	3479	n/a
C03	$t_f + 0.1N_A$	0	389.9	+6.14	1882	-45.9
C04	t_f	5	398.5	n/a	3460	n/a
C05	$t_f + 0.1N_A$	5	420.8	+5.60	1859	-47.9
C06	t_f	10	478.2	n/a	3685	n/a
C07	$t_f + 0.1N_A$	10	501.2	+4.81	2024	-45.1

Given the general direction of flight, the eastern wind leads to a lower ground speed and hence to a longer flight time. However, the number of awakenings -– both the absolute number and the relative improvements -– is not affected significantly. It is noted that the lower ground speed yields a longer exposure time and hence, assuming equal source noise levels, higher SEL values on the ground result. To partly counter this, the initial descent is executed earlier to reduce the headwind component. However, the main explanation for the similar noise impact levels can be explained by considering Fig. 8 which shows the 50.5 dBA SEL contours in which awakenings can occur for cases C03 and C07. This figure reveals that even though nearly the same ground track is being flown – and, although not shown here, the same airspeed and altitude profile – the contour has shifted towards the West. This can readily be explained by considering the effect of wind on noise propagation. In the upwind direction, the wind vector results in a more negative gradient of the speed of sound. Consequently, sound rays will be refracted upward faster, moving the shadow zone closer to the source. In the downwind direction, the wind reduces the negative gradient of the speed of sound gradient or even turns it positive. Consequently, the shadow zone starts farther from the source or is absent as a whole. The consequence is that noise does not propagate ahead of the helicopter as far as in the case without wind, which in this specific case is the most densely populate area. It should also be noted that the effect on the shadow zones is further increased by flying low, again explaining the low altitude flight observed in all cases. This can also be seen in the altitude and airspeed profiles in Fig. 9.
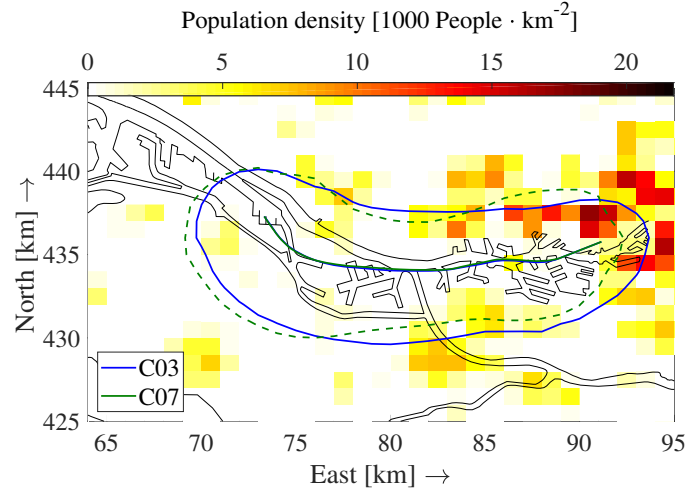
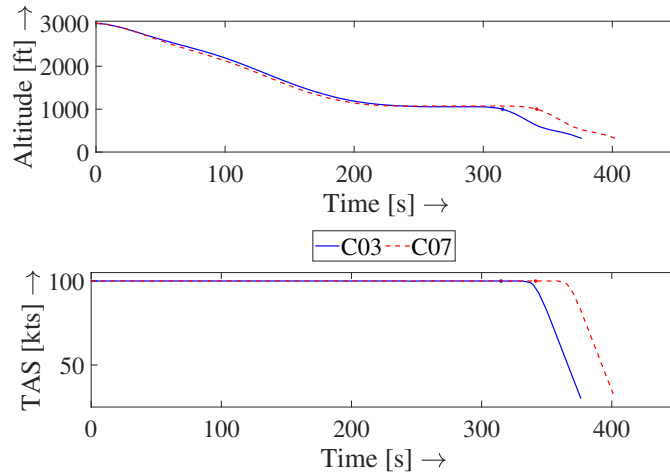**Fig. 8   50.5 dBA SEL contour, cases C03 and C07**

Fig. 9   Altitude and airspeed profile, cases C03 and C07

A final overview of the complete set of cases for all values of k_5 and all wind speeds can be seen in Fig. 10. The figure shows that even though the headwind component significantly affects the flight time, the absolute number of awakenings and the relative gains achievable are hardly affected for all wind conditions considered here.
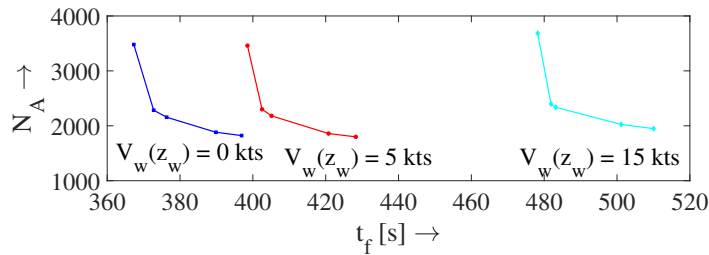

Fig. 10   Flight time vs. awakenings for increasing headwind

To also show the effect of non-standard atmospheric conditions with a different temperature gradient and humidity, an example of an optimization in the conditions of a typical local winter night is given. For this example, the temperature at sea level is set to $-10°$ centigrade with a lapse rate of $+0.001$ K·m^{-1}, and the relative humidity is assumed to be 70%. In these conditions, shadow zones are absent as all sound rays are refracted towards the surface. Numerical results for two cases optimized for minimum time and expected awakenings are presented in Table 4. The table shows that cases C08 and C09 show very similar results – in terms of both absolute numbers and relative changes – as the cases evaluated under ISA conditions. This can readily be explained by considering that even though the atmospheric absorption may be affected by the low temperature, the contribution of absorption to the overall propagation loss is small, especially for the low frequencies considered in this study. The resulting trajectories are not presented here as they closely resemble the trajectories of case C01 and C03

Table 4   Results in ISA and winter conditions

Case	Objective	t_f [s]	Δt_f [%]	N_A	ΔN_A [%]	Conditions
C01	t_f	367.3	n/a	3479	n/a	ISA
C03	$t_f + 0.1N_A$	389.9	+6.14	1882	-45.9	ISA
C08	t_f	367.3	n/a	3305	n/a	Winter
C09	$t_f + 0.1N_A$	394.6	+7.44	1851	-44.0	Winter

As it was found that in all cases discussed above the main driver for the noise mitigation was the increased lateral attenuation, it is also interesting to evaluate the main contributor to the ground effect. The reflection coefficient Q in Eq. (24) is a function of the angle with which the sound ray reaches the ground, the frequency and the ground surface type [?]. As can be seen in Fig. 11, which shows the propagation loss due to absorption and ground effect, the lateral attenuation is highly dependent on the ground surface type. To assess the effect of the ground surface type on helicopter trajectory, a final example is included assuming a tarmac surface (whereas all previous cases assumed a grass surface). Major results are presented in Table 5.

Table 5   Results for different ground surface types

Case	Objective	Ground surface	t_f [s]	Δt_f [%]	N_A	ΔN_A [%]
C01	t_f	Grass	367.3	n/a	3479	n/a
C03	$t_f + 0.1N_A$	Grass	389.9	+6.14	1882	-45.9
C10	t_f	Tarmac	367.3	n/a	5806	n/a
C11	$t_f + 0.1N_A$	Tarmac	393.1	+7.02	4254	-26.7

The table shows a significant change in both the number of awakenings and the achievable noise mitigation resulting from the change in surface conditions. The first is caused directly by the reduced lateral attenuation. Due to the hard ground surface the sound carries further and at comparable slant range to the source higher source noise levels are observed in nearly all observer locations as compared to overflying a grass surface. The reduced lateral attenuation also
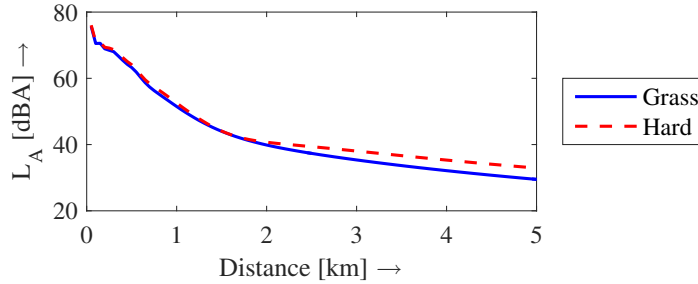
Fig. 11   Sideline noise levels, z = 1,000 ft

explains the fact that the noise impact cannot be reduced by the same degree as when modeling a grass surface. As concluded above, the main means to reduce the noise impact is by flying low and hence increasing the lateral attenuation. Over a hard ground surface lateral attenuation becomes less dominant, and, in fact, spreading losses and absorption gain importance, resulting in a generally slightly higher flight profile for this specific case, as can be observed in Fig. 12.
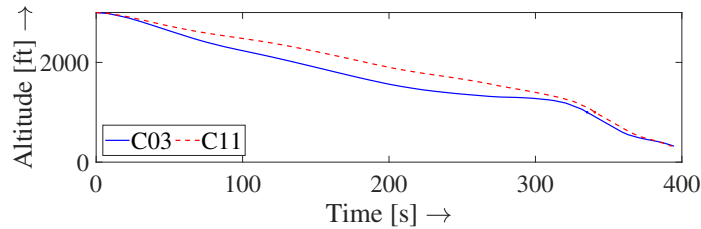
Fig. 12   Altitude profiles over a grass and tarmac surface

VII. Conclusions and Recommendations

The work presented in this paper shows the development of the ECHO software suite, an advanced optimization suite to research green helicopter trajectories developed at Delft University of Technology. It has been shown that the suite can optimize trajectories for a high-fidelity dynamic model of a medium twin-engine helicopter for different criteria and under different atmospheric conditions. It can be concluded that the tool offers an efficient means for solving a complex helicopter optimization problem.

The main focus of the ECHO suite is the identification of noise mitigating trajectories with a strong focus on reducing the noise impact in communities surrounding the heliport. From a number of test cases it was found that in general noise impact reduction has three main drivers. Firstly, by flying at a relatively high airspeed and avoiding steep descents, high source noise levels are avoided. Under these conditions BVI noise is avoided, whereas the occurring HSI noise generally does not reach the populated areas in a sufficient level to cause annoyance. Provided that the peak noise levels directly below the helicopter's flight path are shifted away from noise-sensitive areas, it can be concluded that these flight conditions are in general beneficial to reduce the noise impact. Since most population-based noise impact criteria are based on exposure-based noise metrics, a second effect of the high speed flight is that the exposure time and hence

20

the SEL values are reduced, further reducing the noise impact. The third mitigation strategy follows from the noise propagation losses; in most atmospheric conditions lateral attenuation of noise dominates over the other propagation losses. The lateral attenuation can be increased by reducing the incidence angle between source and receiver, and hence by flying at a lower altitude. The latter effect, however, is highly dependent on the level of propagation losses through absorption, ground effect and spreading. Although not extensively tested, by reducing losses due to the ground by modeling a different ground surface type, a tendency to fly higher was identified, indicating less dominance of the lateral attenuation, and, consequently, a tendency to increase the slant range between source and receiver.

This work gives an initial insight in the means to reduce the helicopter noise impact in populated areas surrounding a helispot. Further case studies are required to analyze in detail the effect of variations in the ambient temperature, relative humidity and wind vector on the noise exposure, and especially on the resulting optimized trajectories. Furthermore, a different noise impact criterion should be considered which is better adapted to the specific helicopter noise characteristics and their impact on the local population. In addition, although the proposed trajectories lead to a significant reduction in the overall noise impact, the noise impact in individual observer locations may be unacceptably high. This could also be accounted for through an alternative noise impact criterion. Finally, the source noise database used in this study is limited to steady-state flight conditions, and only includes the effects of BVI and HSI noise to a limited degree. An extension of the source noise database would lead to a better insight on the impact of these effects.

Acknowledgments

References